Supplemental information:

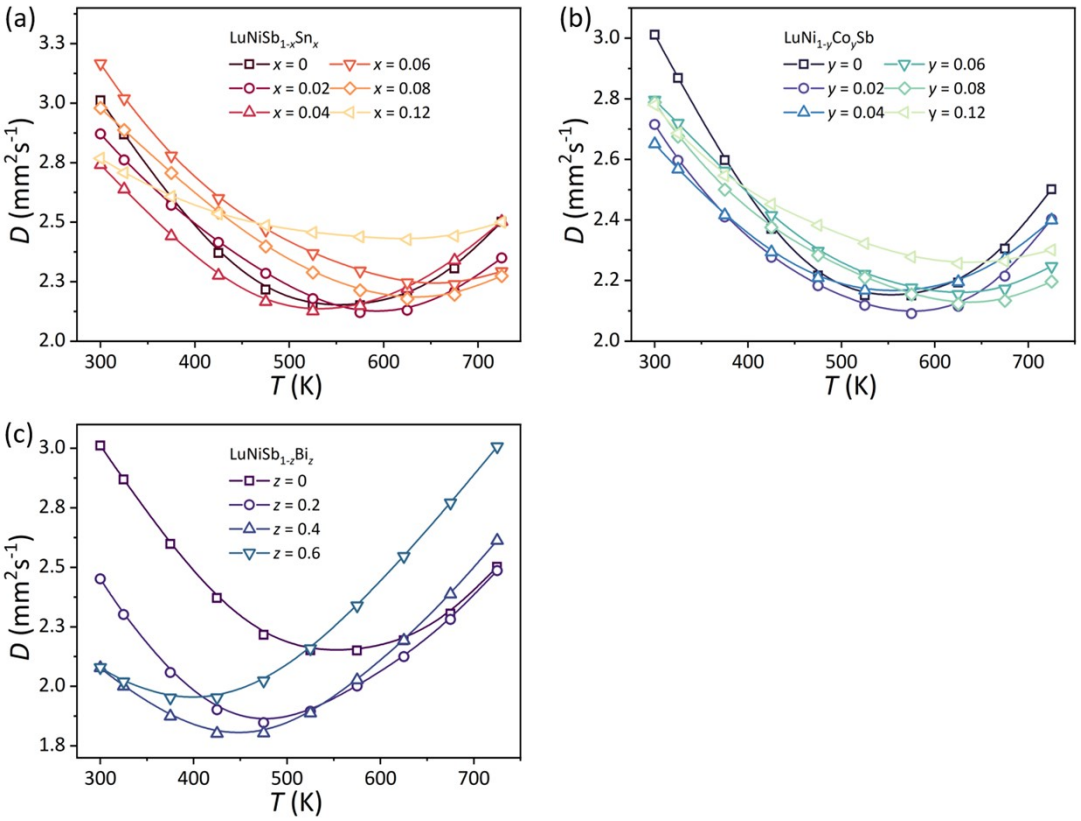

Fig. S1. (a) Thermal diffusivity D of (a) $LuNiSb_{1-x}Sn_x$, (b) $LuNi_{1-y}Co_ySb$ and (c) $LuNiSb_{1-z}Bi_z$.

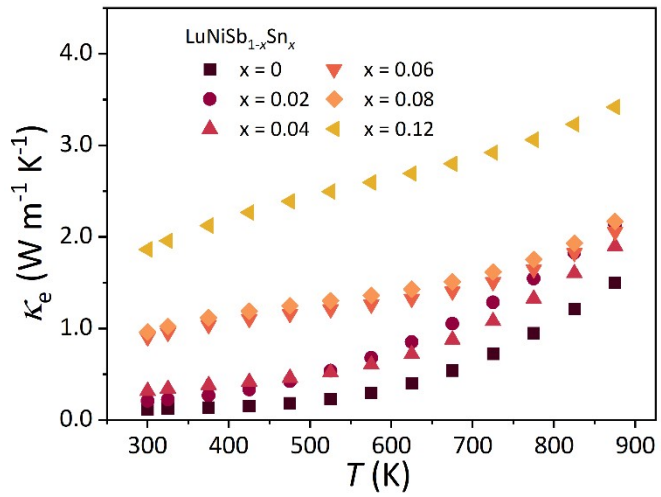

Fig. S2. The electronic thermal conductivity of $LuNiSb_{1-x}Sn_x$.

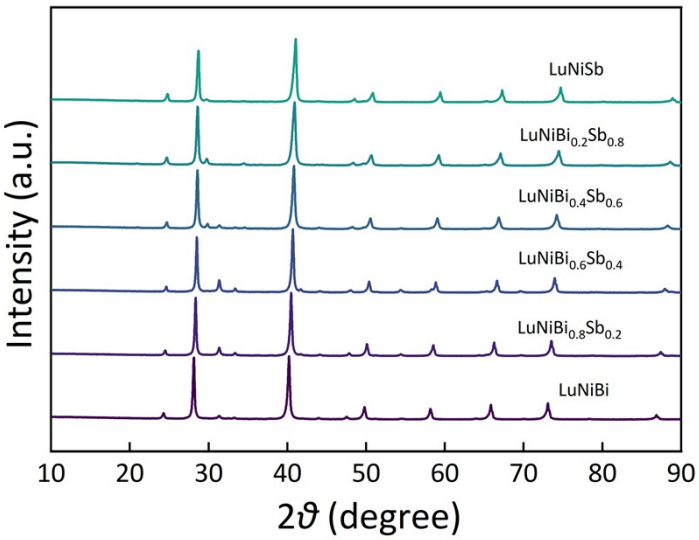

Fig. S3. The XRD patterns at room temperature for $LuNiSb_{1-z}Bi_z$.

Eq. S1. The model proposed by Klemens and Abeles:

$$\tau_{\mathrm{D}}^{-1} = \tau_{\mathrm{M}}^{-1} + \tau_{\mathrm{S}}^{-1} = \frac{V_0 \omega^4}{4\pi v_{\mathrm{s}}^3}(\Gamma_M + \Gamma_{\mathrm{S}})$$

Where V_0 is the volume of the unit cell, ω is the frequency, v_{s} is the average velocity of the bulk, Γ_{M} and Γ_{S} are the disordered factors of mass and stress field fluctuations, respectively. When atoms are doped at a single position in one compound, the disorder parameters can be written as:

$$\Gamma_M \propto f_i^1 f_i^2 (\frac{M_i^1 - M_i^2}{\overline{M_i}})^2 \text{ and } \Gamma_S \propto f_i^1 f_i^2 \varepsilon_i (\frac{r_i^1 - r_i^2}{\overline{r_i}})^2$$

where, f_i^{k} is the percentage of components, ε_i is a relevant parameter of elasticity, which is always assigned at the range of two orders of magnitude for HH materials. M_i^1, M_i^2, and $\overline{M_i}$ are the atomic mass of host, dopant, and weighted average of *i* compound. Identically, r_i^1, r_i^2, and $\overline{r_i}$ are the radius of the counterpart.

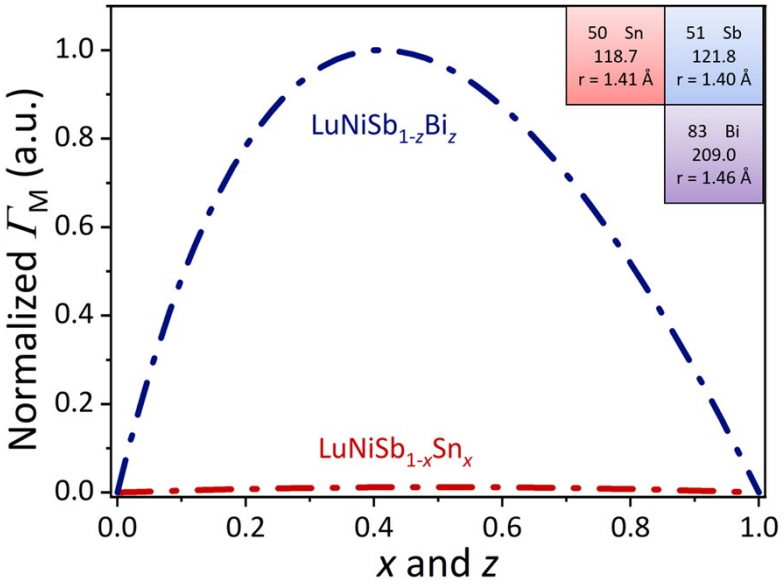

Fig. S4. The normalized relative disorder *vs*. the concentration of Sn doping or Bi alloying.

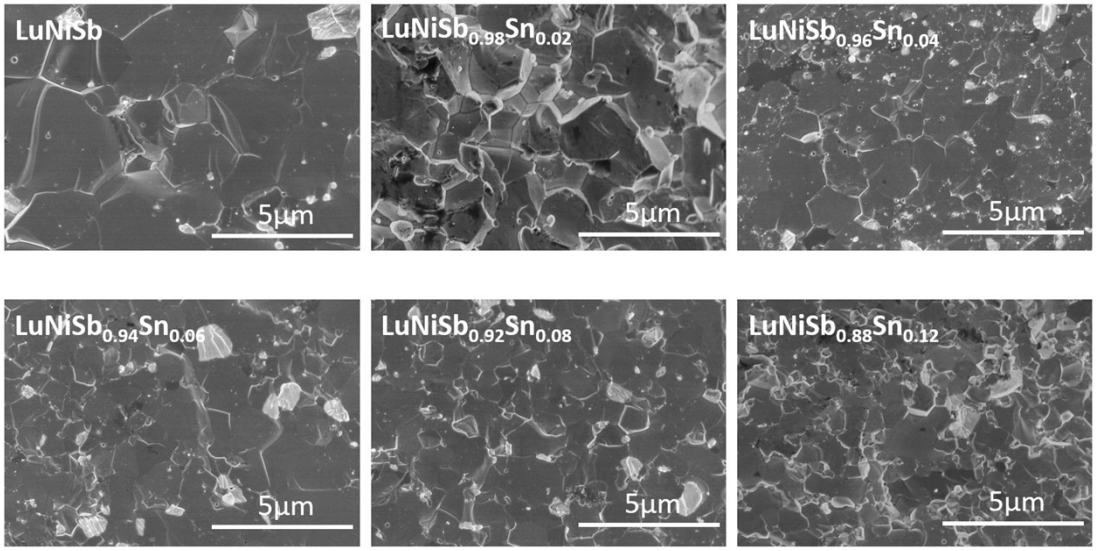

Fig. S5. The morphology of fracture surface for $LuNiSb_{1-x}Sn_x$.

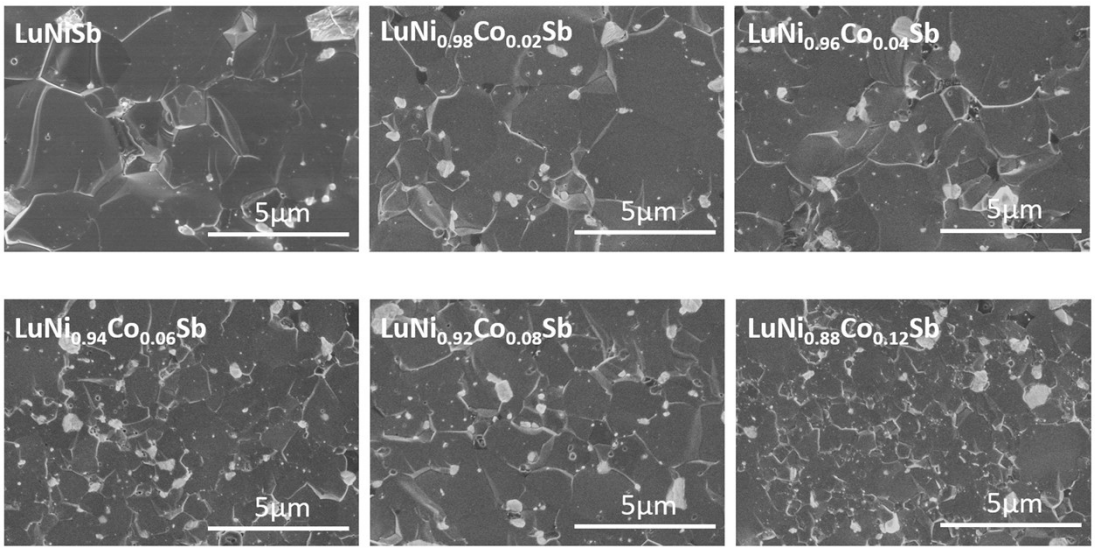

Fig. S6. The morphology of fracture surface for $LuNi_{1-y}Co_ySb$.

Supplementary Note 1:

The morphology of the fracture surface of LuNiSb indicates that its grain size is on the order of ~ 5 μm, and under the same synthesis process, when the doping concentration of Sn and Co reaches 12%, the grain size decreases to ~ 1 μm (Fig. S5 and S6). Although grain boundary might result in additional scattering of phonons, the effect of its scattering strength is far less significant than other scattering mechanisms, and its specific scattering rate can be written as:

$$\frac{1}{\tau_B} = \frac{v_s}{L}$$

Where v_s is the average velocity and L is the average grain size. With further sound velocity measurements, it is found that the v_s of the samples hardly changes with the increased doping

concentration (Table S1). When v_s = 3350 m/s and L = 5 μm are brought into the above equation, the grain boundary scattering rate of 6.7×10^{-4} THz will be obtained. Even if the grain boundary is reduced to 1 μm, this scattering is on the order of 10^{-3} THz, which is insignificant compared to the other scattering mechanisms (Fig. S8).

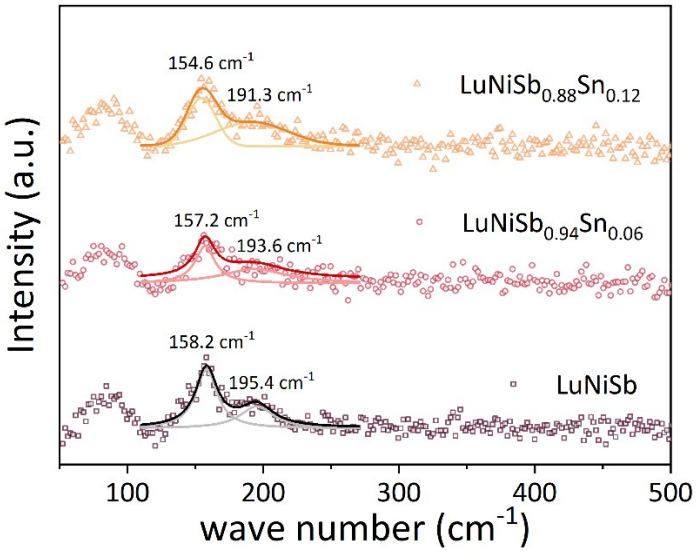

Fig. S7. Raman spectra for LuNiSb, $LuNiSb_{0.94}Sn_{0.06}$, and $LuNiSb_{0.88}Sn_{0.12}$.

Table S1. The transverse v_t, longitudinal v_l and average velocity v_s for $LuNiSb_{1-x}Sn_x$ and $LuNi_{1-y}Co_ySb$.

$LuNiSb_{1-x}Sn_x$	v_t (m/s)	v_l (m/s)	v_s (m/s)
$x = 0$	2585	4500	3349
$x = 0.02$	2561	4468	3320
$x = 0.04$	2557	4528	3328
$x = 0.06$	2591	4560	3367
$x = 0.08$	2595	4556	3370
$x = 0.12$	2565	4495	3330

$LuNi_{1-y}Co_ySb$	v_t (m/s)	v_l (m/s)	v_s (m/s)
$y = 0$	2585	4500	3349
$y = 0.02$	2594	4495	3357
$y = 0.04$	2581	4577	3361
$y = 0.06$	2585	4604	3370
$y = 0.08$	2600	4588	3381
$y = 0.12$	2548	4602	3334

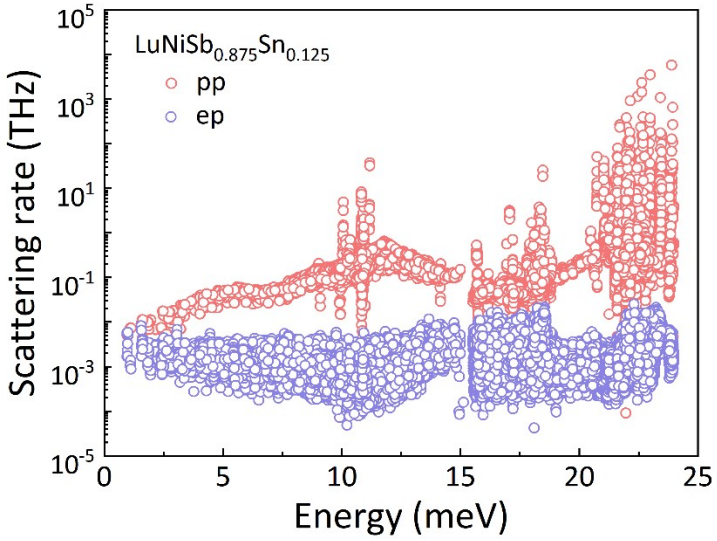

Fig. S8. The scattering rate of p-p and e-p for $LuNiSb_{0.875}Sn_{0.125}$.

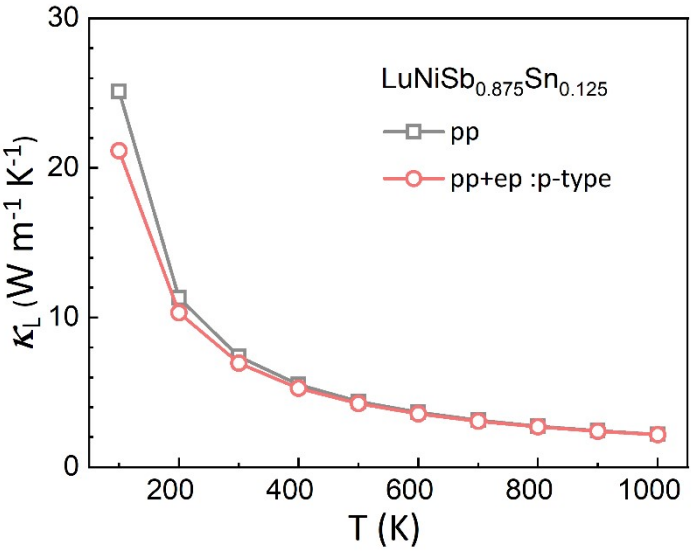

Fig. S9. The calculated temperature-dependent κ_L of $LuNiSb_{0.875}Sn_{0.125}$ by only considering p-p or both p-p and e-p.

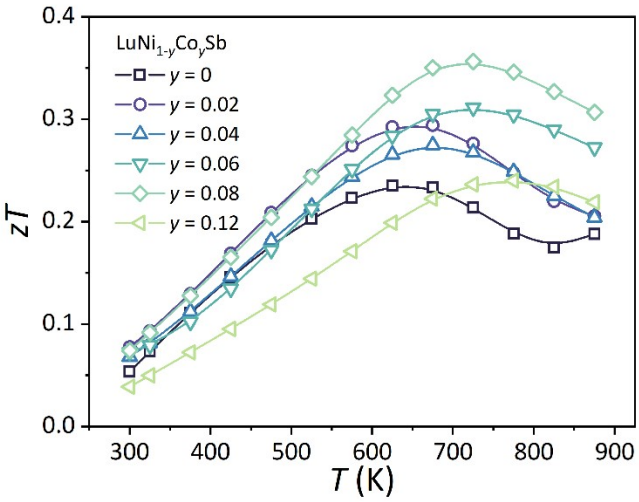

Fig. S10. Temperature dependence of zT for $LuNi_{1-y}Co_ySb$.